www.czasopisma.pan.pl PAN www.journals.pan.pl
Archives of Acoustics Vol. 47, No. 2, pp. 223–240 (2022), doi: 10.24425/aoa.2022.141652

Research Paper

Evaluation of the Acoustic Performance of Porous Materials Lined Ducts with Geometric Discontinuities

Dhouha TOUNSI[(1)], Wafa TAKTAK[(2)], Raja DHIEF[(1),(3)], Mohamed TAKTAK[(1),(3)*], Mabrouk CHAABANE[(3)], Mohamed HADDAR[(1)]

[(1)] *Mechanics, Modelling and Production Laboratory (LA2MP)*
Mechanical Department, National School of Engineers of Sfax, University of Sfax
Sfax, Tunisia
*Corresponding Author e-mail: mohamed.taktak@fss.rnu.tn

[(2)] *National School of Engineers of Sfax, University of Sfax*
Sfax, Tunisia

[(3)] *Faculty of Sciences of Sfax*
Sfax, Tunisia

(*received December 27, 2020; accepted February 7, 2022*)

Duct silencers provide effective noise reduction for heating, ventilation and air conditioning systems. These silencers can achieve an excellent sound attenuation through the attributes of their design. The reactive silencer works on the principle of high reflection of sound waves at low frequencies. On the other hand, the dissipative silencer works on the principle of sound absorption, which is very effective at high-frequencies. Combining these two kinds of silencers allowed covering the whole frequency range. In this paper, the effect of liner characteristics composed of a perforated plate backed by a porous material and geometry discontinuities on the acoustic power attenuation of lined ducts is evaluated. This objective is achieved by using a numerical model to compute the multimodal scattering matrix, thus allowing deducing the acoustic power attenuation. The numerical results are obtained for six configurations, including cases of narrowing and widening of a radius duct with sudden or progressive discontinuities. Numerical acoustic power attenuation shows the relative influence of the variation in the values of each parameter of the liner, and of each type of radius discontinuities of ducts.

Keywords: geometric discontinuities in duct systems; acoustic impedance; porous materials; perforated plate; acoustic power attenuation.

1. Introduction

Duct silencers provide effective noise reduction for heating, ventilation and air conditioning systems. Lined duct attenuators are an example of these silencers. This is the most effective and efficient method that is widely used to reduce noise in such kinds of ducts systems. Acoustic liners are based on the use of acoustic absorbent materials such as porous materials, Helmholtz resonators or perforated plates. In order to obtain great acoustic power attenuation, these elements can be combined together and coupled with sudden or progressive section change of the duct to increase the acoustic performance of the lined duct element.

To characterize the acoustic behavior of duct discontinuities with rigid wall and lined parts, numerous methods were proposed like the work of Miles (1946), Peat (1988a; 1988b), Munjal (1987), Kergomard and Garcia (1987), Amir *et al.* (1996) and Selamet *et al.* (2004). To evaluate the acoustic performance of ducts systems, different matrices were used such as the transfer matrix (Peat, 1988a; Munjal, 1987; Craggs, 1989), reflection matrix (Akoum, Ville, 1998; Sitel *et al.*, 2003), transmission matrix (Sitel *et al.*, 2003) or multimodal scattering matrix (Åbom, 1991; Leroux *et al.*, 2003; Bi *et al.*, 2006; Sitel *et al.*, 2006). The latter matrix showed its efficiency in modeling duct elements and liner impedance at higher-order modes. In fact, such matrix presents an intrinsic pro-

priety of the duct element: it depends only on acoustic and geometric features of the duct. The method to compute this matrix was performed by Taktak *et al.* (2008; 2010; 2012), Kessentini *et al.* (2016) and Ben Souf *et al.* (2017) in the case of axisymmetric duct with and without flow. Then, this method was improved to evaluate the effect of the temperature on the acoustic impedance of lined duct, see (Benjedidia *et al.*, 2014).

In a previous work, Othmani *et al.* (2015) used this method to evaluate the effect of liner characteristics on the acoustic power attenuation of lined duct, then Masmoudi *et al.* (2017) investigated the effect of geometry and impedance on the acoustic behavior of wall and porous material lined duct but using the simple model of Delany-Bazely which depends only on the flow resistivity. This was carried out for two configurations of duct diameter increase and duct diameter decrease with liner composed of a porous material and a perforated plate. Recently, Dhief *et al.* (2020) treated the problem of duct discontinuities with more complicated configurations and using liners composed of perforated plates backed by air cavity or porous materials. They showed that the second type of liner is more efficient in absorbing acoustic waves than the first one.

The present work presents a continuation of this work: the effect of porous material and perforated plate characteristics parameters of the liner on the acoustic power attenuation of various ducts discontinuities configurations is investigated in details to evaluate the efficacy of each parameter composing this liner by a numerical model to compute the multimodal scattering matrix. From this matrix, the acoustic power attenuation is computed. This objective is achieved by studying six configurations of cylindrical ducts, presenting cases of narrowing and widening of a radius duct with sudden or progressive discontinuities.

The outline of the paper is organized as follows: in Sec. 2, the description of the physical problem and the numerical computation of the multimodal scattering matrix is presented. Section 3 presents the computation of the acoustic power attenuation. Section 4 presents the used acoustic impedance of the liner. Finally, numerical results are presented and discussed in Sec. 5, to evaluate the influence of liner characteristics on the acoustic power attenuation of each studied configuration.

2. Description of the problem and numerical computation of the scattering matrix

In this paper, a rigid-lined-rigid cylindrical duct is studied. It is located between two axial coordinates z_R and z_L with 1 m in length and radius $a = R/\rho$ at these positions. Six configurations of ducts with geometric discontinuities are under consideration in this paper. They differ according to the type of variation of discontinuity and position of the liner.

Figures 1 and 2 present the symmetric parts of narrowing and widening portion of the studied ducts. The acoustic impedance of the liner is made of a perforated plate, backed by absorbing porous material before the rigid wall (Fig. 3), modeled by its acoustic impedance Z. The change of the section is located between z_1 and z_2. The duct radius change is equal to 0.02 m.

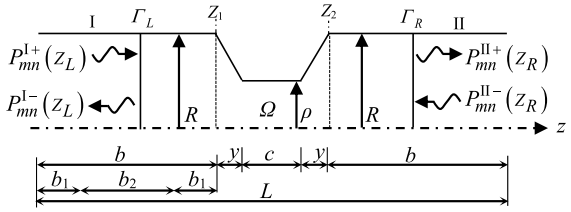

Fig. 1. Duct presenting a narrowing in the duct radius.

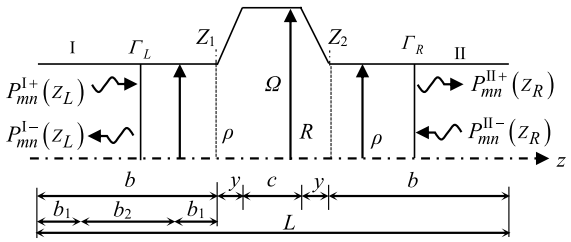

Fig. 2. Duct presenting a widening in the duct radius.

For the case of duct presenting radius narrowing (Fig. 1), the duct radius R is equal to 0.075 m. Three configurations are studied which differ with respect to the type of discontinuities and the position of the liner:

(I-a) $y = 0$: sudden narrowing and the part c is lined;

(I-b) $y \neq 0$: progressive narrowing and the part c is lined;

(I-c) $y = 0$: sudden narrowing and the part b_2 is lined. The length of the duct is $L = b_1 + b_2 + b_1 + b + c$.

For the case of duct presenting widening of the radius (Fig. 2) characterized by a radius ρ equal to 0.055 m, three configurations are studied, which differ with regard to the type of discontinuities and the position of the liner:

(II-a) $y = 0$: sudden widening and the part c is lined;

(II-b) $y \neq 0$: progressive widening and the part c is lined;

(II-c) $y = 0$: sudden widening and the part b_2 is lined. The length of the duct is equal to $L = b_1 + b_2 + b_1 + b + c$.

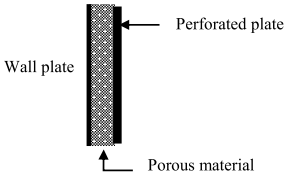

Fig. 3. Composition of the studied liner.

The multimodal scattering matrix $\mathbf{S}_{2N\times 2N}$ of the duct element located between the axial coordinates z_L (L meaning left-side) z_R (R meaning right side) relates the outcoming pressure waves array

$$\mathbf{P}_{2N}^{\text{out}} = \left\langle P_{00}^{\text{I}-}(z_L), ..., P_{mn}^{\text{I}-}(z_L),\ P_{mn}^{\text{II}+}(z_R), ..., P_{mn}^{\text{II}+}(z_R)\right\rangle_{\text{N}}^{\text{T}}$$

to incoming pressure waves array

$$\mathbf{P}_{2N}^{\text{in}} = \left\langle P_{00}^{\text{I}+}(z_L), ..., P_{mn}^{\text{I}+}(z_L),\ P_{mn}^{\text{II}-}(z_R), ..., P_{mn}^{\text{II}-}(z_R)\right\rangle_{\text{N}}^{\text{T}}$$

as follows, see (Åbom, 1991; Taktak *et al.*, 2010):

$$\mathbf{P}_{2N}^{\text{out}} = \mathbf{S}_{2N\times 2N} \times P_{2N}^{\text{in}}, \tag{1}$$

where $\left(P_{mn}^{\text{I}+}, P_{mn}^{\text{I}-}\right)$ and $\left(P_{mn}^{\text{II}+}, P_{mn}^{\text{II}-}\right)$ are, respectively, the modal pressure coefficients associated to the (m, n) mode traveling, respectively, in the positive and the negative direction in both regions I and II (Figs 1 and 2); m and n are the azimuthal and the radial mode numbers, respectively; N is the number of propagating modes in both cross sections. The acoustic pressure p in the axisymmetric duct is obtained by solving the Helmholtz equation with the boundary conditions, respectively, at Γ_{WD} with rigid wall duct and at Γ_{LD} with lined duct part, characterized by its acoustic impedance:

$$\begin{cases} \Delta p + k^2 p = 0 & (\Omega), \\ Z\dfrac{\partial p}{\partial n_{LD}} = i\omega\rho_0 p & (\Gamma_{LD}), \\ \dfrac{\partial p}{\partial n_{WD}} = 0 & (\Gamma_{WD}), \end{cases} \tag{2}$$

where Δ is the Laplacian operator, Ω is the acoustic domain inside the duct, $\mathbf{n}_W$ and $\mathbf{n}_L$ correspond to normal vectors of each wall, k is the total wave number, ρ_0 is the mass per volume unit, and ω is the angular frequency.

To solve the system of Eqs (2), the finite element method is used. The corresponding weak variational formulation can be written as:

$$\Pi = -\int_{\Omega} (\nabla q \cdot \nabla p)\, \mathrm{d}\Omega + k^2 \int_{\Omega} qp\, \mathrm{d}\Omega + \int_{\cup\Gamma_i} q\frac{\partial p}{\partial n_i}\, \mathrm{d}\Gamma_i = 0, \tag{3}$$

where q is the test function, $\mathrm{d}\Omega$ and $\mathrm{d}\Gamma_i$ are integration elements through the duct domain and boundaries, respectively, and $\cup\Gamma_i$ presents the whole boundary ($i = LD$ (lined part), L (left), R (right)). The use of modal decomposition at boundaries (Γ_R and Γ_L) introduces the modal pressures as additional degrees of freedom of the model. This is performed by supposing that pressures at Γ_L and Γ_R can be obtained by the projection of the acoustic field over the eigen functions of the rigid wall duct:

$$\begin{aligned} \int_{\Gamma_L} pJ_m\left(\frac{\chi_{mn}}{a}r\right)\mathrm{d}\Gamma_L &= \left(P_{mn}^{\text{I}+} + P_{mn}^{\text{I}-}\right) \cdot \int_{\Gamma_L} J_m\left(\frac{\chi_{mn}}{a}r\right)^2 r\, \mathrm{d}\Gamma_L, \\ \int_{\Gamma_R} pJ_m\left(\frac{\chi_{mn}}{a}r\right)\mathrm{d}\Gamma_R &= \left(P_{mn}^{\text{II}+} + P_{mn}^{\text{II}-}\right) \cdot \int_{\Gamma_R} J_m\left(\frac{\chi_{mn}}{a}r\right)^2 r\, \mathrm{d}\Gamma_R, \end{aligned} \tag{4}$$

where r is the radial coordinate.

The last integral of the formulation (3) is given by the following expression, by adding the modal incoming and outcoming pressures as additional degrees of freedom to the model:

$$\begin{aligned} \int_{\cup\Gamma_i} q\frac{\partial p}{\partial n}\, \mathrm{d}\Gamma &= \int_{\Gamma_t} q\left(\frac{i\omega\rho p}{Z}\right)\mathrm{d}\Gamma_{LD} \\ &+ \sum_{n}^{N_r} ik_{mn}\left[\left(n_L\left(P_{mn}^{\text{I}+} - P_{mn}^{\text{I}-}\right)\int_{\Gamma_L} qJ_m(\chi_{mn}r)\, \mathrm{d}\Gamma_L\right)\right. \\ &+ \left.\left(n_R\left(P_{mn}^{\text{II}+} - P_{mn}^{\text{II}-}\right)\int_{\Gamma_R} qJ_m(\chi_{mn}r)\, \mathrm{d}\Gamma_R\right)\right], \end{aligned} \tag{5}$$

where J_m is the Bessel function of the first kind of order m, χ_{mn} is the n-th root satisfying the radial hard-wall boundary condition on the wall of the main duct ($J'(\chi_{mn}/a) = 0$).

For a fixed m, system (3) results in the following matrix system, by taking into account the boundary conditions (Taktak *et al.*, 2010):

$$\left[[q_1, ..., q_M], [1, ..., 1]\right]\begin{bmatrix} \mathbf{K} & \mathbf{E}_1 & \mathbf{E}_2 & \mathbf{F}_1 & \mathbf{F}_2 \\ \mathbf{G}_1 & \mathbf{G}_2 & \mathbf{G}_3 & 0 & 0 \\ 0 & 0 & 0 & 0 & 0 \\ 0 & 0 & 0 & 0 & 0 \\ \mathbf{H}_1 & 0 & 0 & \mathbf{H}_2 & \mathbf{H}_3 \end{bmatrix} \cdot \begin{Bmatrix} \begin{Bmatrix} p_1 \\ \vdots \\ p_M \end{Bmatrix} \\ P_{mn}^{\text{I}-} \\ P_{mn}^{\text{I}+} \\ P_{mn}^{\text{II}-} \\ P_{mn}^{\text{II}+} \end{Bmatrix} = \begin{Bmatrix} 0 \\ \vdots \\ 0 \end{Bmatrix}, \tag{6}$$

where M is the node number in the domain Ω, $\{p\}$ is the nodal acoustic pressure vector, $\mathbf{K}$ is a matrix relating the test function to the nodal pressures in the

domain, $\mathbf{E}_1$, $\mathbf{E}_2$, $\mathbf{F}_1$, and $\mathbf{F}_2$ are matrices relating the test function to the modal pressures on Γ_L and Γ_R, $\mathbf{G}_1$, $\mathbf{G}_2$, and $\mathbf{G}_3$ are matrices relating the nodal acoustic pressures in Ω to different modal pressures on the boundary Γ_L, $\mathbf{H}_1$, $\mathbf{H}_2$, and $\mathbf{H}_3$ are matrices relating the nodal acoustic pressures to different modal pressures on the boundary Γ_R.

The azimuthal scattering matrix is written as:

$$\mathbf{s} = \left(\mathbf{V} - \mathbf{C}\,\mathbf{K}^{-1}\mathbf{B}^{-1}\right)\left(\mathbf{U} - \mathbf{C}\,\mathbf{K}^{-1}\mathbf{A}^{-1}\right), \tag{7}$$

where $\mathbf{A}$, $\mathbf{B}$, $\mathbf{C}$, $\mathbf{U}$, and $\mathbf{V}$ are defined as:

$$\mathbf{A} = [\mathbf{E}_1 \;\; \mathbf{F}_2], \qquad \mathbf{B} = [\mathbf{E}_2 \;\; \mathbf{F}_1], \qquad \mathbf{C} = \mathbf{G}_1 + \mathbf{H}_1,$$
$$\mathbf{U} = [\mathbf{G}_2 \;\; \mathbf{H}_3], \qquad \mathbf{V} = [\mathbf{G}_3 \;\; \mathbf{H}_2]. \tag{8}$$

The total scattering matrix of the studied ducts $\mathbf{s}_{2Nr\times 2Nr}$ is obtained by repeating this operation for each m and by assembling the azimuthal matrices $s_{2Nr\times 2Nr}$ with N is the total number of modes present in the ducts.

3. Computation of the acoustic power attenuation

The acoustic power attenuation W_{att} of a two-port duct is developed by (Aurégan, Starobinski, 1999). It connects the acoustic power on both sides of the incoming waves W_{in} and the outgoing waves W_{out} with the following expression:

$$W_{\text{att}}\;[\text{dB}] = 10\log\frac{W^{\text{in}}}{W^{\text{out}}} = 10\log\left(\frac{\sum_{i=1}^{2N}|d_i|^2}{\sum_{i=1}^{2N}\lambda_i\,|d_i|^2}\right). \tag{9}$$

These total energies can be expressed in the following form:

$$W^{\text{in}} = \sum_{m=-P}^{P}\sum_{n=0}^{Q}\frac{N_{mn}}{2\rho_0 c_0}\left(\frac{k^+_{mn}}{k}\left|P^{\text{I+}}_{mn}\right|^2 + \frac{k^-_{mn}}{k}\left|P^{\text{II-}}_{mn}\right|^2\right), \tag{10}$$

$$W^{\text{out}} = \sum_{m=-P}^{P}\sum_{n=0}^{Q}\frac{N_{mn}}{2\rho_0 c_0}\left(\frac{k^-_{mn}}{k}\left|P^{\text{I-}}_{mn}\right|^2 + \frac{k^+_{mn}}{k}\left|P^{\text{II+}}_{mn}\right|^2\right), \tag{11}$$

with $N_{mn} = SJ(\chi_{mn})\left(1-\frac{m^2}{\chi_{mn}}\right)$ associated to the mode $(m,\,n)$, $S = \pi a^2$ is the cross section area, and $k_{mn} = S\sqrt{k^2 - \left(\frac{\chi_{mn}}{a}\right)^2}$ is the axial wave number of mode $(m,\,n)$ in the main duct, d_i and λ_i are the components and the eigenvalues of the matrix $\mathbf{H}$ defined as:

$$\mathbf{H}_{2N\times 2N} = \left[\mathbf{XO}_{2N\times 2N}\mathbf{S}_{2N\times 2N}\mathbf{XI}^{-1}_{2N\times 2N}\right]^{\text{T}^*}_{2N\times 2N} \cdot\left[\mathbf{XO}_{2N\times 2N}\mathbf{S}_{2N\times 2N}\mathbf{XI}^{-1}_{2N\times 2N}\right]_{2N\times 2N} \tag{12}$$

with

$$XI_{mn} = \left[\text{diag}\left(\sqrt{N_{mn}k^+_{mn}/2\rho_0 c_0 k}\right)\right]_{2N\times 2N},$$
$$XO_{mn} = \left[\text{diag}\left(\sqrt{N_{mn}k^-_{mn}/2\rho_0 c_0 k}\right)\right]_{2N\times 2N},$$
$$\mathbf{d}_{2N} = \mathbf{U}^{\text{T}^*}_{2N\times 2N}\mathbf{\Pi}^{\text{in}}_{2N},$$

where $\mathbf{U}$ is the eigenvectors of $\mathbf{H}$ and T^* denotes conjugate transpose.

4. Modeling of the liner

The acoustic impedance of the liner composed of a perforated plate and an absorbing porous material backed by a rigid plate is obtained as follows:

$$Z = Z_{\text{porous material}} + Z_{\text{perforated plate}} \tag{13}$$

with

$$Z_{\text{porous material}} = Z_c \cdot \coth(jk_c d). \tag{14}$$

Z_c and k_c are the surface characteristic impedance and propagation constant of the porous material, respectively, and d is the material depth. The values of Z_c and k_c are estimated by the Lafarge-Allard model (Allard, Attalla, 1993; Lafarge *et al.*, 1997), expressed as follows:

$$Z_c = \omega\sqrt{\rho_m K}, \tag{15}$$

$$k_c = \omega\sqrt{\frac{\rho_m}{K}}, \tag{16}$$

where K is the compressibility and ρ_m is the density of the fluid saturating the porous medium rigid structure as defined by Allard and Attalla (1993) and Lafarge *et al.* (1997) as follows:

$$\rho_m = \alpha_\infty\rho_0\left[1 - j\frac{\sigma\phi}{\rho_0\alpha_\infty\omega}\sqrt{1 + \frac{4j\rho_0\alpha^2_\infty\omega\eta}{\sigma^2\phi^2\Lambda^2}}\right], \tag{17}$$

$$K = \gamma P_0\left[\gamma - \frac{(\gamma-1)}{1 + \frac{\eta\phi}{j\omega\rho_0 N_{pr}k'_0}\sqrt{1 + \frac{4j\omega\rho_0 N_{pr}(k'_0)^2}{\eta\phi^2\Lambda'^2}}}\right], \tag{18}$$

where α_∞ and ϕ are the material tortuosity and porosity, respectively, σ is the material flow resistivity, ρ_0 is the air density, ω is the angular frequency ($\omega = 2\pi f$) with f is the frequency, η is the dynamic viscosity, γ is the ratio of specific heats at, respectively, constant pressures C_p and volumes C_v defined as follows:

$$\gamma = \frac{C_p}{C_v}, \tag{19}$$

where N_{Pr} is the Prandtl number, η is the dynamic viscosity, Λ and Λ' are the viscous and thermal characteristic lengths, respectively, P_0 is the atmospheric pressure, and k'_0 is the thermal permeability.

For the perforated plate, many models exist in the literature to model its impedance (Elnady, Boden, 2004; Lee, Selamet, 2006; Wang *et al.*, 2017;

Tiryakioglu, 2020). In this paper, the acoustic impedance model of Elnady and Boden (2004) is used:

$$Z_E = \mathrm{Re}\left\{\frac{ik}{\sigma_p C_D}\left[\frac{t}{F\left(k'_s d_p/2\right)}+\frac{\delta_{\mathrm{Re}}}{F\left(k_s d_p/2\right)}\right]\right\} + i\,\mathrm{Im}\left\{\frac{ik}{\sigma_p C_D}\left[\frac{t}{F\left(k'_s d_p/2\right)}+\frac{\delta_{\mathrm{Im}}}{F\left(k_s d_p/2\right)}\right]\right\} \quad (20)$$

with C_D being the discharge coefficient, d_p is the pore diameter, t is the plate thickness, σ_p is the plate porosity, δ_{Re} and δ_{Im} are correction coefficients given as follows:

$$\delta_{\mathrm{Re}} = 0.2d_p + 200d_p^2 + 16000d_p^3,$$

$$\delta_{\mathrm{Im}} = 0.2856d_p,$$

$$F\left(k_s d_p/2\right) = 1 - \frac{J_1\left(k_s d_p/2\right)}{k_s \frac{d_p}{2} J_0\left(k_s d_p/2\right)},$$

$$F\left(k'_s d_p/2\right) = 1 - \frac{J_1\left(k'_s d_p/2\right)}{k'_s \frac{d_p}{2} J_0\left(k'_s d_p/2\right)}, \quad (21)$$

$$k'_s = \sqrt{\frac{-i\omega}{\nu'}},$$

$$k_s = \sqrt{\frac{-i\omega}{\nu}},$$

where $\nu' = 2.179\frac{\eta}{\rho_0}$ is the kinematic viscosity.

5. Numerical results

The characteristics of the propagation medium (the air), the porous material and the perforated plate are listed in Table 1. The used porous material is the industrial material "Acusticell" (Sagartzazu, Hervella-Nieto, 2008). The studied frequency range is $ka = [0, 3.8]$ (ka is the Helmholtz number and $N = 5$ modes are propagating $[(0,0),(\pm1,0),(\pm2,0)]$.

The acoustic impedance is used as an input for computation of the numerical multimodal scattering matrix of the studied ducts and therefore the acoustic power attenuation is calculated.

5.1. Study of several combinations of absorbent materials

The acoustic parameters of six porous materials of acusticell, aluminum, melamine, rockwool, CP-01, and MP-10 and the three perforated plates properties are indexed in Tables 1 and 2, respectively.

Table 1. Values of the of perforated plate properties.

Parameter	Plates		
	P1	P2	P3
Thickness t [m]	0.001	0.0008	0.0008
Hole diameter d [m]	0.001	0.001	0.0003
Porosity σ [%]	2.5	5	5
Discharge Coefficient C_D	0.76	0.76	0.76

5.1.1. Porous materials proprieties effects

Figure 4 presents the acoustic power attenuation of configuration (I-a) of duct with sudden narrowing radius versus ka using the acusticell (M1), aluminum (M2), melamine (M3), rockwool (M4), CP-01 (M5), and MP-10 (M6) porous material and the perforated plate (P1). It can noted that the form of attenuation curves changes when the depth is equal to 24 mm. Results show that the attenuation reaches its maximum, for ka varying from 3 to 3.4 for M1, M2, M3, and M4 and for ka = 1.8 for M5 and M6. The amplitude of this maximum is about 4 dB, 4.4 dB, 5.8 dB, 6.3 dB, and 6.8 dB for M2, M3, and M4, M5, M6, and M1, respectively. It can be clearly seen that acoustic atte-

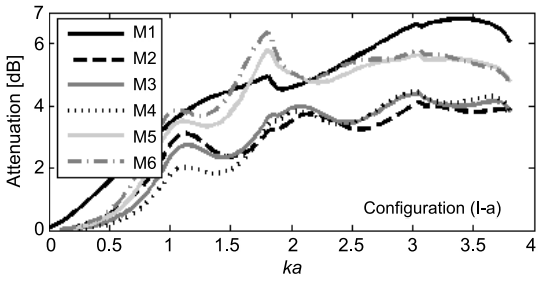

Fig. 4. Acoustic power attenuation of the configuration (I-a) of duct having sudden radius narrowing for several studied porous materials with the perforated plate P1.

Table 2. The porous materials proprieties (Mereze *et al.*, 2012).

Parameter	Acusticell M1	Aluminium M2	Melamine M3	Rockwool M4	CP-01 M5	MP-10 M6
Depth d [m]	0.024	0.0126	0.011	0.01	0.01	0.0098
Flow resistivity σ [N·s/m^4]	22000	4700	10300	20600	202000	364000
Porosity φ [%]	95	84	99	98	68	60
Tortuosity α_∞ [–]	1.38	1.08	1.0	1.01	2.2	2.3
Char. viscous length Λ [m]	170.10^{-6}	348.10^{-6}	128.10^{-6}	90.10^{-6}	54.10^{-6}	40.10^{-6}
Char. thermal length Λ' [m]	510.10^{-6}	175.10^{-6}	120.10^{-6}	85.10^{-6}	33.10^{-6}	26.10^{-6}

nuation is greatly linked to both the depth and the flow resistivity. In considering only the depth, the acoustic attenuation very slightly grows with the increase of depth (~1.1 dB) in the range of frequencies ka = [0.8, 1.5] for M2, M3, and M4 and out of that range, the attenuation curves of these porous materials are almost similar, knowing that the viscous characteristic lengths pass from 90 μm to 348 μm. By increasing the depth to d = 24 mm, the acoustic power attenuation reaches a maximum, except that, in the intervals ka = [0.9, 1.1] and in the interval ka = [1.5, 2.1], where the attenuation can be more efficient according to the greater values of flow resistivity. Consequently, the acoustic power attenuation is significantly affected if the flow resistivity and the depth are increasing considerably.

Figure 5 shows that the acoustic power attenuation of configuration (I-a) of duct with sudden widening radius versus ka using the acusticell (M1), aluminum (M2), melamine (M3), rockwool (M4), CP-01 (M5) and MP-10 (M6) and the perforated plate (P1). It can be observed that the levels of acoustic power attenuation are greatly enhanced when compared to the case of configuration (I-a). Results show that the attenuation is maximum at ka = 1.8 for M1, near to ka = 2.9 for M2, M3, and M4, and for ka = 3.8 for M5 and M6. The amplitude of this maximum is about 6.3 dB, 7.2 dB, 7.9 dB, 10.7 dB, 10.7 dB, and 11.5 dB for M2, M3, M4, M1, M6, and M5, respectively. It can be seen that the attenuation curves of M2, M3, and M4 have the same shape and they are very close for ka near 2.5 then they are slightly increasing with the increase of the flow resistivity and the viscous characteristic lengths. It is remarkably seen that the attenuation is very high especially at higher frequencies for M5 and M6 due to great airflow resistivity. It is noticeable that the attenuation related to d = 24 mm has its maximum at the low-frequency zone until ka = 2 and then, the attenuation is better related to the higher values of flow resistivity. Thus, it can be concluded that the higher depth (d = 24 mm) is better to enhance the attenuation particularly in low-frequency region and the flow resistivity can be more efficient especially in high-frequency region. So, the flow resistivity and the depth are considered to be effective for improved acoustic attenuation.

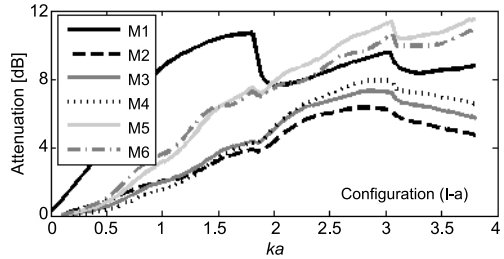

Fig. 5. Acoustic power attenuation of the configuration (I-a) of duct having sudden radius widening for several studied porous materials with the perforated plate P1.

5.1.2. Perforated plates proprieties effects

The acoustic power attenuation of the configuration (I-a) for three porous materials covered with three perforated plates is illustrated in Fig. 6. It can be noted that the decrease of the porosity generates an increase of acoustic attenuation for the three porous materials. By considering only the porosity, a maximum of attenuation passes from 6 dB for the M1.P2 to 6.8 dB for the M1.P1 and $W_{\mathrm{att,max}}$ = 3.6 dB for the M2.P2 to $W_{\mathrm{att,max}}$ = 4.3 dB for the M2.P1 and $W_{\mathrm{att,max}}$ = 3.1 dB for the M3.P2 to $W_{\mathrm{att,max}}$ = 4 dB for the M3.P1. The decrease of the porosity is considered to be effective for increasing acoustic attenuation. It can be seen that the attenuation very slightly grows with the decrease of the plate hole diameter except for ka above 3.05 for M1.P1 when compared to perforated plates P2 and P3.

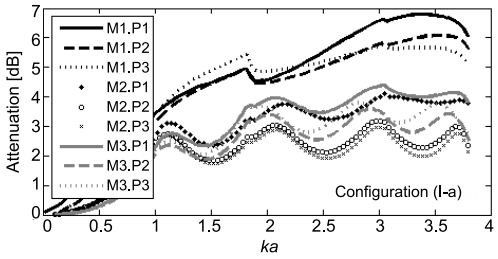

Fig. 6. Acoustic power attenuation of the configuration (I-a) of duct having sudden radius widening for several used porous materials and perforated plates.

Figure 7 shows the acoustic power attenuation of the configuration (II-a) for three porous materials covered with three perforated plates. Results show that the variation of the attenuation is changed for all three porous materials according to the proprieties of perforated plates. It is seen for ka above 1.5, that the attenuation grows as the decrease of the porosity for the first porous material, where the maximum of attenuation passes from 9.6 dB for M1.P to 10.3 dB for M1.P2 at ka = 3. For M2 and M3 porous materials, the maximum of attenuation varies: $W_{\mathrm{att,max}}$ = 7.3 dB for M2.P1 to $W_{\mathrm{att,max}}$ = 4.6 dB for M2.P2 and $W_{\mathrm{att,max}}$ = 6.3 dB for M3.P1 to $W_{\mathrm{att,max}}$ = 4.2 dB for M3.P2. Considering only the plate hole diameter, it is observed that the decrease of the hole diameter of the plate generates an increase of the attenuation for all three porous ma-

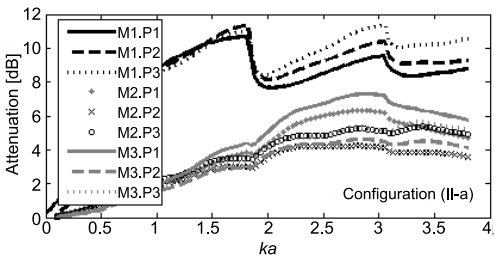

Fig. 7. Acoustic power attenuation of the configuration (II-a) for several perforated plates coupled with three used porous materials.

terials when compared P2 and P3 perforated plates: $W_{att,max}$ = 7.3 dB for M1.P2 to $W_{att,max}$ = 4.6 dB for M12.P3 and $W_{att,max}$ = 6.3 dB for M2.P2 to $W_{att,max}$ = 4.2 dB for M2.P3 and $W_{att,max}$ = 6.3 dB for M3.P2 to $W_{att,max}$ = 4.2 dB for M3.P3. It is concluded that the plate porosity has a significant influence on the attenuation.

5.2. Parametric study

The only models used to estimate the acoustic impedance of the perforated plate and the porous material for evaluating the effects of the liner characteristics are respectively P1 and Acusticell (M1). The effect of nine parameters is studied by varying one parameter and leaving the others fixed.

5.2.1. Configurations of ducts having a radius narrowing

Plate characteristics effects. Figure 8 shows the effect of the plate thickness on the acoustic power attenuation, respectively, for configurations (I-a), (I-b), and (I-c) versus *ka*. These figures indicate that the acoustic power attenuation increases, as a function of frequency *ka*; however, a drop can be noticed at the first mode cut-on frequency in Fig. 8a as well as in Fig. 8b, where the attenuation exhibits drop at the mode cut-on frequencies. It is observed that the variation of the plate thickness from 0.5 to 8 mm has an effect in Figs 8a and 8b, however, it has no significant effect in Fig. 8c with small variation at higher frequencies which does not exceed 2 dB. It can be seen that the more plate is thick the attenuation is greater. This growing of the attenuation appears in Fig. 8a for *ka* ranging from to 0.7 to 2.7, especially at *ka* =1.8 the (1,0) cut-on frequency. The maximum attenuation passes from 4.6 dB for t = 0.5 mm to 7 dB for t = 8 mm at *ka* = 1.8. With reference to Fig. 8b, the increase of the attenuation appears in the interval of *ka* = [1, 1.8] and *ka* = [2.5, 3]. The maximum attenuation passes from 6.8 dB for t = 0.5 mm to 10 dB for t = 8 mm in *ka* = 1.8, and from 8.1 dB for t = 0.5 mm to 11 dB for t = 8 mm in *ka* = 3.05. The observed effect is explained by the fact that the mass of air contained in the perforation is more important when the plate is thicker. Acoustic resistance increases with increasing plate thickness and the thermal and viscous boundary layers in the perforations are present on a larger surface. The acoustic dissipation is, therefore, more important. The attenuation drops being a reflection of a filtering higher order modes: mode conversion phenomenon. It is found that the frequency of peak attenuation where the thickness can affect significantly remains identical regardless of t, around to attenuation drops. This implies that filtering the modes is related to the duct radius. In fact, by changing the radius, the modal distribution varies and consequently the conversion phenomena between the modes.

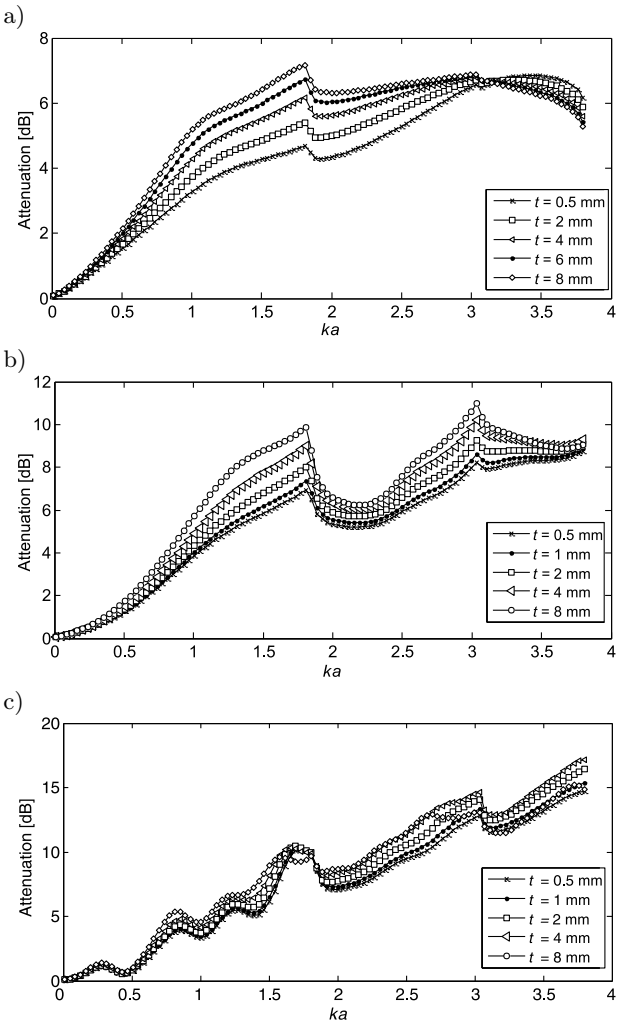

Fig. 8. Effect of the plate thickness t [mm] on the acoustic power attenuation for ducts of the three studied configurations versus *ka*: a) (I-a), b) (I-b), and c) (I-c).

As shown in Figs 8a and 8b, the attenuation of configuration (I-a) is close to the configuration (I-b) but with less abrupt variations. The level of attenuation of the configuration (I-c) differs from others due to liner position change. Results show that maximum attenuation and the corresponding frequency change in each studied configuration and they are about 7.1 dB at *ka* = 1.8, 10.97 dB at *ka* = 3.03, and 17.1 dB at *ka* = 3.8 for configurations (I-a), (I-b), and (I-c), respectively. This leads to say that the configuration (I-c), having a lined part before a sudden radius narrowing, is more absorbent and also more efficient than configurations (I-a) and (I-b).

Figure 9 displays the effect of the perforation diameter of the perforated plate on the acoustic power attenuation of ducts respectively of configurations (I-a), (I-b), and (I-c) versus *ka*. Results show that this parameter has a significant effect. It can be noted that the attenuation curves changed in the same form for

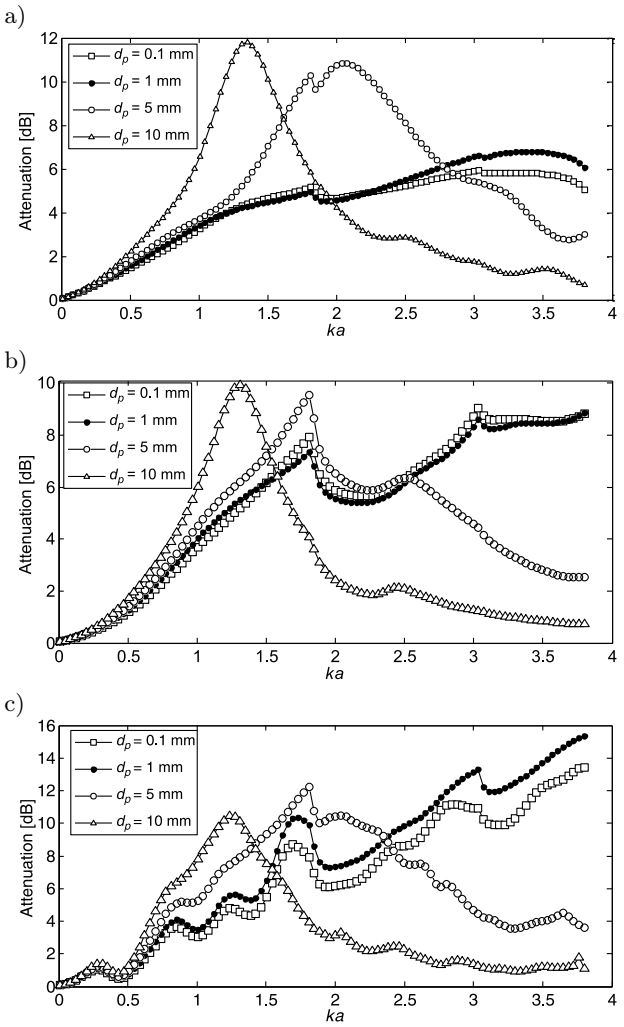

Fig. 9. Effect of the hole diameter diameter d_p [mm] of the perforated plate on the acoustic power attenuation of the three studied configurations: a) (I-a), b) (I-b), and c) (I-c).

all three studied configurations, when varying the hole diameter d_p, from 0.1 mm to 10 mm.

The results related to d_p = 0.1 and 1 mm are very close, indicating that the attenuation curves increase to the final point when ka increases, with drops at the mode cut-on frequencies, as shown in Fig. 9b. The maximum of acoustic power attenuation varies significantly from each configuration and it changes as follows:

- for d_p = 0.1 mm, the maximum attenuation is about 6 dB, 9 dB, and 13.3 dB for configurations (I-a), (I-b), and (I-c), respectively;
- for d_p = 1 mm, this maximum is about 6.8 dB, 9 dB, and 15.3 dB for configurations (I-a), (I-b), and (I-c), respectively.

Based on the results obtained from d_p = 5 mm to 10 mm, it can be noted that the attenuation curves present peaks, whose amplitudes and corresponding frequencies increase when d_p increases, except for that in Fig. 9c, which displays a slight decrease of the amplitude. In addition, it is observed that the frequency band becomes narrower. These peaks are formed with larger diameters, giving rise to a resonance peak-type in the acoustic attenuation at medium frequency. Smaller diameters do not make it possible to highlight this phenomenon (not showing resonance peak attenuation). This is attributed to the fact that the diameter is too small, and therefore the acoustic waves are reflected from the plate instead of entering through the absorbing material. For d_p = 10 mm, results show that the attenuation reaches a maximum near ka equal 1.3 and the amplitude of this maximum is about 12 dB, 10.4 dB, and 10.8 dB for configurations (I-a), (I-b), and (I-c), respectively. According to the results of attenuation, it can be concluded that configuration (I-c) is more absorbent than configurations (I-b) (~5 dB) and (I-b) (~3 dB). Thus, configuration (I-c) is the most efficient.

Figure 10 displays the effect of the variation of the plate porosity on the acoustic power attenuation

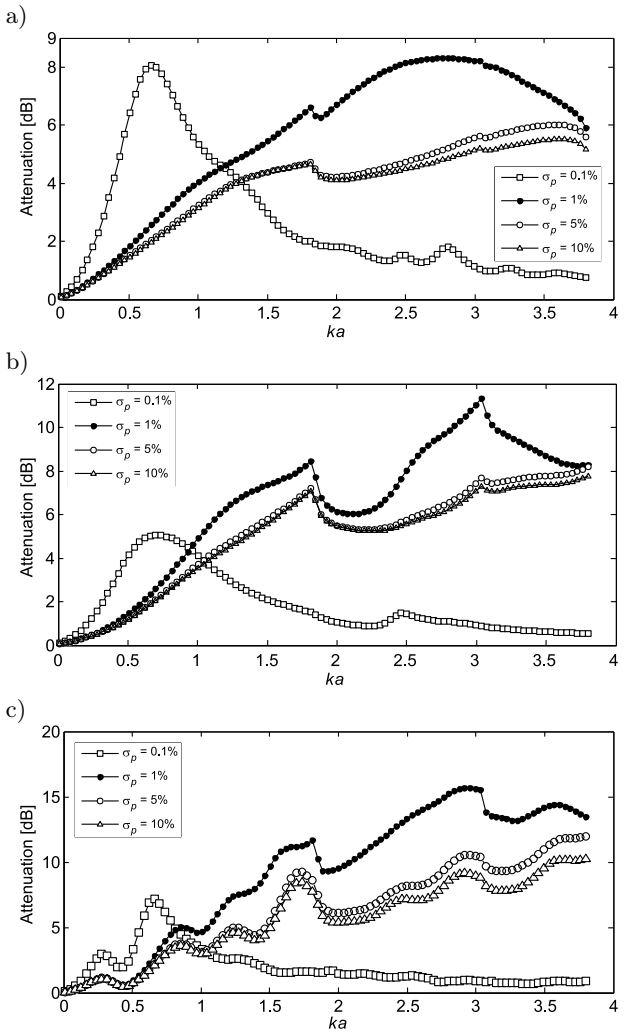

Fig. 10. Effect of porosity σ_p [%] of the perforated plate on the acoustic power attenuation of the three studied configurations: a) (I-a), b) (I-b), and c) (I-c).

respectively for the configurations (I-a), (I-b), and (I-c) versus *ka*. It is noteworthy that the effect of σ_p in all three figures is almost similar, and significant as well. With the exception of σ_p = 0.1%, It can be observed that the attenuation increases with the frequency *ka*, however, it slightly decreases for high frequencies (*ka* above 3) in Fig. 10a and it drops at the mode cut-on frequencies in Fig. 10b. Increasing the porosity generates a decrease of acoustic attenuation and remains almost close for σ_p = 5, 10%. For σ_p = 0.1%, the acoustic power attenuation shows a peak at low frequency $ka \in [0.5, 1]$ and it is relatively small (~<2 dB) outside that range. The amplitude of this peak is about 8 dB, 5 dB, 7.1 dB for configurations (I-a), (I-b), and (I-c), respectively. Results show clearly that σ_p = 1% is more efficient in terms of enhancing the acoustic attenuation of major parts of curves. A maximum of attenuation is about 8.2 dB, 11.3 dB, and 15.6 dB in the range of $ka = [2.8, 3]$ for configurations (I-a), (I-b), and (I-c), respectively. Accordingly, configuration (I-c) with porosity 1% is the most efficient and it can be a reasonable choice from an acoustical design point of view.

Material porous properties effects. The effect of the flow resistivity (σ) on the acoustic power attenuation versus *ka* for the three studied configurations (I-a), (I-b), and (I-c) are presented in Fig. 11. Results show that the variation of acoustic power attenuation, in all studied configurations, is similar to that of the effect of thickness in Fig. 8; however, the attenuation curves of Fig. 11c are slightly disturbed. It is observed that the attenuation reaches its maximum for *ka*, varying from 3 to 3.8. The amplitude of this maximum is about 7.8 dB, 10 dB, and 15.6 dB for configurations (I-a), (I-b), and (I-c), respectively. According to these figures it can be concluded that increasing the flow resistivity from 10^3 N·s/m^4 to 10 000 N·s/m^4 has no effect. The variation of the acoustic power attenuation is negligible. On the other hand, increasing σ to the values of $5 \cdot 10^4$ N·s/m^4 and 10^5 N·s/m^4 generates an increase of acoustic attenuation, except for that at *ka* above 2.1, where attenuation varies inversely in Fig. 11a, and for $\sigma = 10^5$ N·s/m^4 in Fig. 11c, which presents a small decrease at *ka* above 1.5. This increase is more apparent near the first mode cut-on frequency in Figs 11a and 11b about ~4 dB, while it does not exceed 3 dB in Fig. 11c. This can be elucidated by the increase of the thermal and viscous dissipations of each configuration, when the flow resistivity of the material increases. It is concluded that configuration (I-c) is the most efficient, particularly at high frequencies, thus the material of $\sigma = 5 \cdot 10^4$ N·s/m^4 is an appropriate choice.

Figures 12–14 exhibit, respectively, the effect of the variation of the thermal permeability, the tortuosity, and the porosity of the porous material on the acoustic power attenuation versus *ka* for the configurations

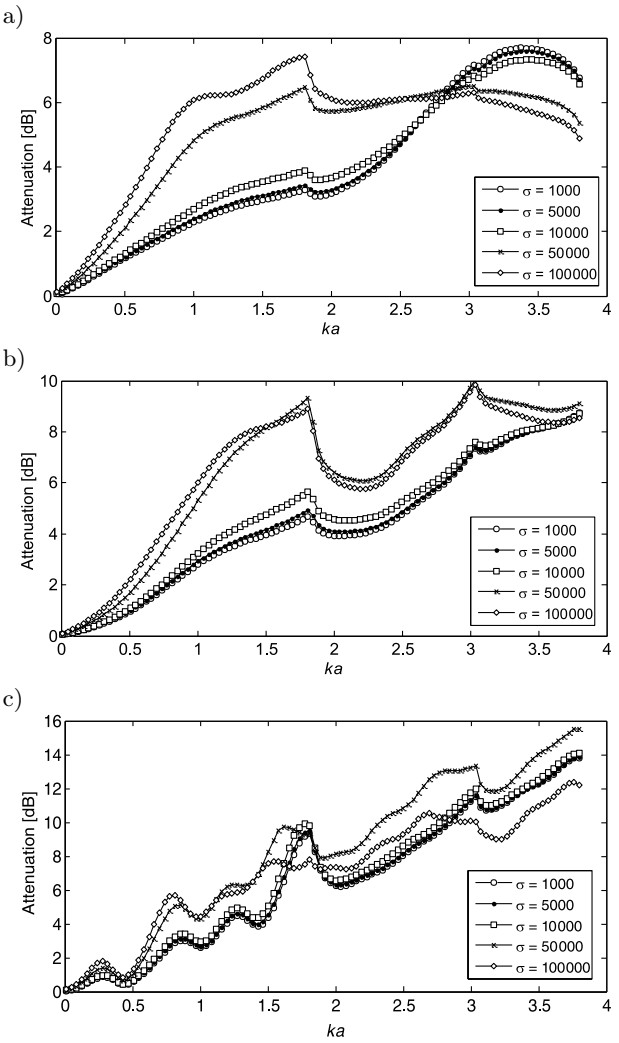

Fig. 11. Effect of the flow resistivity σ [N·s/m^4] of the porous material on the acoustic power attenuation of the three studied configurations: a) (I-a), b) (I-b), and c) (I-c).

(I-a), (I-b), and (I-c), respectively. These figures show that the three parameters of porous material k_0', α_∞, and ϕ give close results and the variation of the attenuation is almost the same for each of the studied configuration. The attenuation behavior for each configuration can be described as follows: the acoustic power attenuation gradually increases when *ka* rises, however, showing a very little decrease near to *ka* = 1.8 and it slightly reduces again from *ka* = 3.05, the second cut-on frequency in configuration (I-a) as well as configuration (I-b) but the drops at the mode cut-on frequencies are higher and a very small fluctuations are observed in configuration (I-c). The effect of these parameters is evaluated by varying: the thermal permeability from 10^{-7} to 10^{-10}, the tortuosity α_∞ from 1 to 2.5, and the porosity ϕ from 0.5 to 0.9. The values variation of each of these parameters shows that there is no significant effect on the acoustic attenuation. Figure 12 shows that the variation of the attenuation is negligible and it does not exceed 2 dB. A ma-

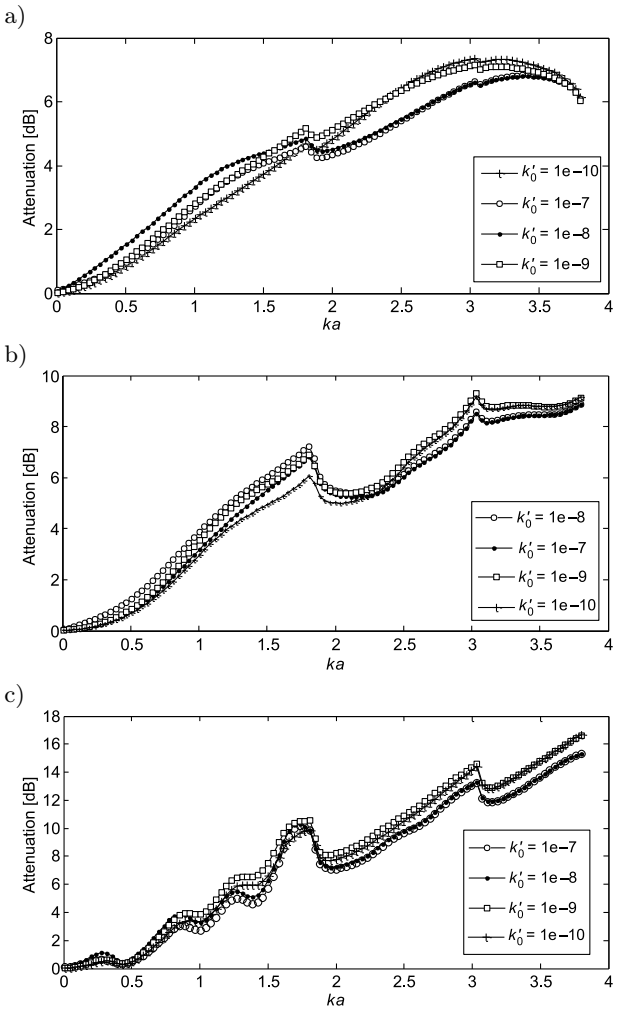

Fig. 12. Effect of the thermal permeability k_0' [m^2] of the porous material on the acoustic power attenuation of the three studied configurations: a) (I-a), b) (I-b), and c) (I-c).

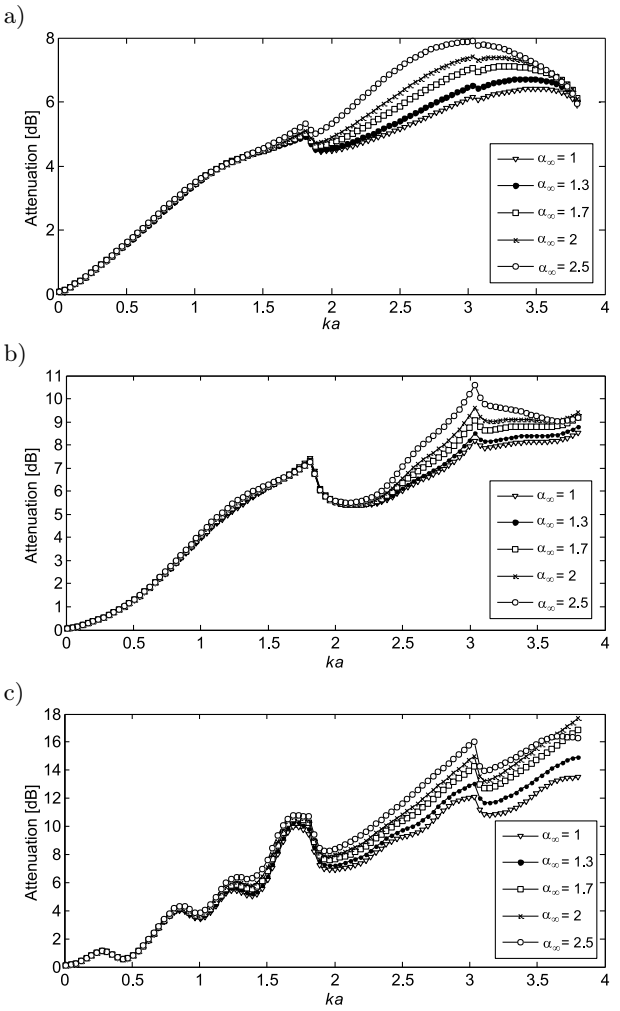

Fig. 13. Effect of tortuosity α_∞ of the porous material on the acoustic power attenuation of the three studied configurations: a) (I-a), b) (I-b), and c) (I-c).

ximum of attenuation is noted for ka greater than 3, being about 7.5 dB, 9 dB, and 17 dB for configurations (I-a), (I-b), and (I-c), respectively. Figure 13 also shows that there is no effect of the tortuosity on attenuation for ka below 1.9 in Figs 13a and 13c, and for ka below 2.3 in Fig. 13b. However, above these values of ka, the attenuation increases slightly when α_∞ increases. For Figs 13a and 13b, the increase of the acoustic power attenuation is smaller to 2 dB but it passes from 13.2 dB for $\alpha_\infty = 1$ to 16.3 dB for $\alpha_\infty = 2.5$ at $ka = 3.6$ in Fig. 13c. It is concluded that tortuosity α_∞ has a low effect only for higher frequencies, since it describes the inertial effects in the high frequencies. The attenuation reaches a maximum for values of ka ranging between [3, 3.8]. This maximum is about 8 dB, 10.5 dB, and 16.4 dB for configurations (I-a), (I-b), and (I-c), respectively. Figure 14 indicates that the effect of the porosity is not important, with small increases of attenuation as the porosity increases in the range of $ka = [1, 2.5]$ in Figs 14a and 14b. Results show that the attenuation reaches a maximum for values of ka ranging between (3.5, 3.8). A maximum of attenuation varies for each configuration: (I-a): 7.4 dB; (I-b): 8.8 dB; (I-c): 15.4 dB. It can be concluded from these results that the effect of these parameters is not significant because they are found in a quite small porous layer and therefore, the effects: inertial, viscous and thermal between fluid and structure are low. It is noticeable also that configuration (I-c) is more efficient compared to configurations (I-a) and (I-b), it yields a better attenuation for the three Figs 12, 13, and 14.

Figure 15 represents the effect of viscous characteristic length (Λ) on the acoustic power attenuation versus ka for configurations (I-a), (I-b), and (I-c), respectively. These figures reveal that this parameter has a remarkable effect and the attenuation curves in all three configurations vary, with similar form. By varying length Λ from 10^{-3} to 10^{-6}, the effect of this parameter was evaluated in all three figures: it is shown that the low values of Λ (from 10^{-3} to 10^{-4}) has no effect on the attenuation and the variation of attenu-

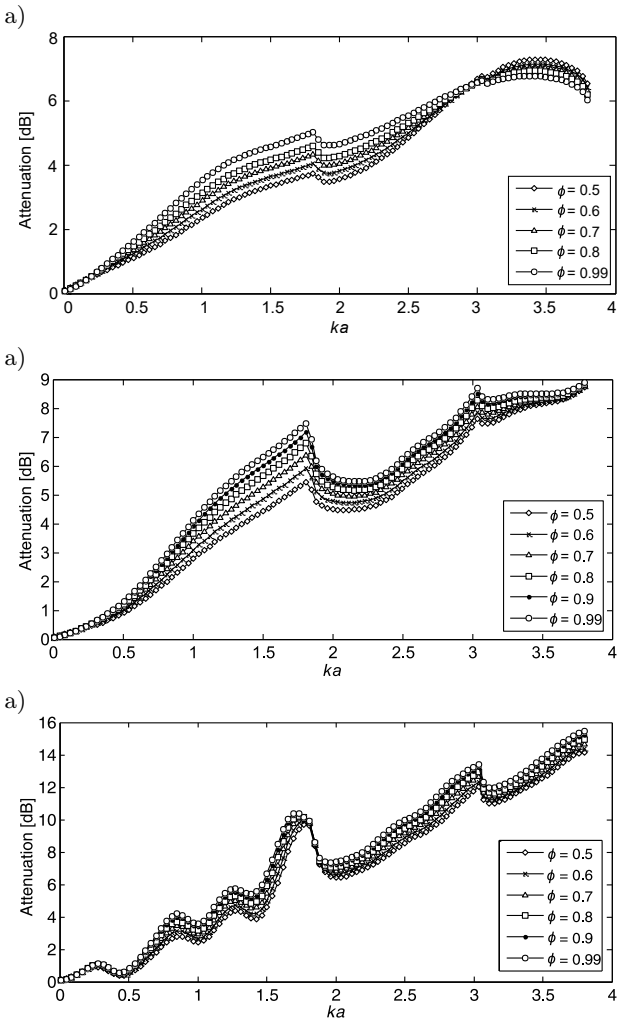

Fig. 14. Effect of the porosity ϕ of the porous material on the acoustic power attenuation of the three studied configurations: a) (I-a), b) (I-b), and c) (I-c).

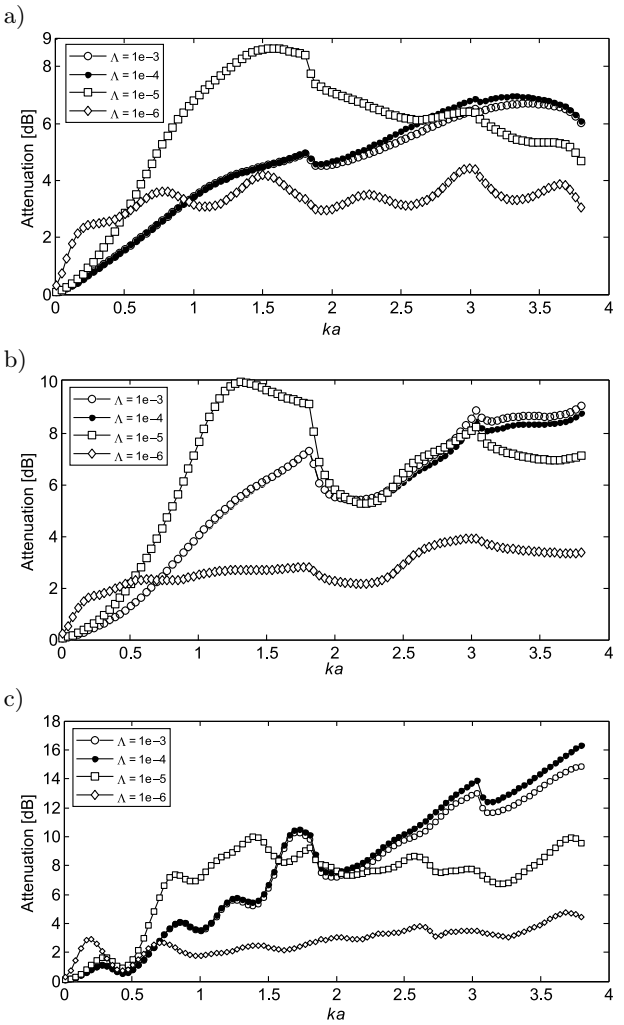

Fig. 15. Effect of the characteristic viscous length Λ [m] of the porous material on the acoustic power attenuation of the three studied configurations: a) (I-a), b) (I-b), and c) (I-c).

ation curves is similar to the thermal permeability effect k_0'. Increasing this parameter to 10^{-5} generates an increase of the attenuation for ka below 2.6 in Figs 15a and 15b (which presents a maximum of attenuation), as well as in Fig. 15c for ka below 1.55. It is observed that increasing Λ to 10^{-6} generates strong decreases of the attenuation in all configurations, which remain almost at the same line. The maximum attenuation and the corresponding frequencies vary for each figure as follows: (I-a): 8.8 dB at $ka = 1.6$ for $\Lambda = 10^{-5}$; (I-b): 10 dB at $ka = 1.4$ for $\Lambda = 10^{-5}$; (I-c): 16.1 dB at $ka = 3.8$ for $\Lambda = 10^{-4}$. According to these results, it can be concluded that configuration (I-c) is the most absorbent, with the value of $\Lambda = 10^{-5}$, being good at low frequency region and that related to $\Lambda = 10^{-3}$ and $\Lambda = 10^{-4}$ can be more efficient at high frequency region.

Figure 16 represent the effect of the depth of the porous material on the acoustic power attenuation versus ka, respectively, for configurations (I-a), (I-b), and (I-c). These figures show that this parameter has a significant effect. The increase of the depth d from 0.01 m to 0.08 m introduces an increase of the acoustic attenuation into each configuration. The attenuation curves became very close for the values $d = 0.06$, 0.08 m. The increase of the frequency increases the attenuation in all studied configurations, with small variations: It can be seen that Figs 16a and 16b, which differ on the type of discontinuity, yield close results with a slight difference, manifested by a drop at the mode cut-on frequencies in Fig. 16b, which has a slightly more important maximum of attenuation (~3 dB). As expected, configuration (I-c) exhibits a slight perturbation, while having a better attenuation than the other configurations. The maximum of attenuation and the corresponding frequencies vary with respect to each figure as follows: (I-a): 3.8 dB at $ka = 3.6$ for $d = 0.01$, and 8.4 dB at $ka = 1.8$ for $d = 0.08$; (I-b): 4.7 dB at $ka = 3.8$ for $d = 0.01$, and 11.2 dB at $ka = 3$ for $d = 0.08$; and (I-c): 3.8, 5 dB for $d = 0.01$, and 16.5 dB for $d = 0.08$.

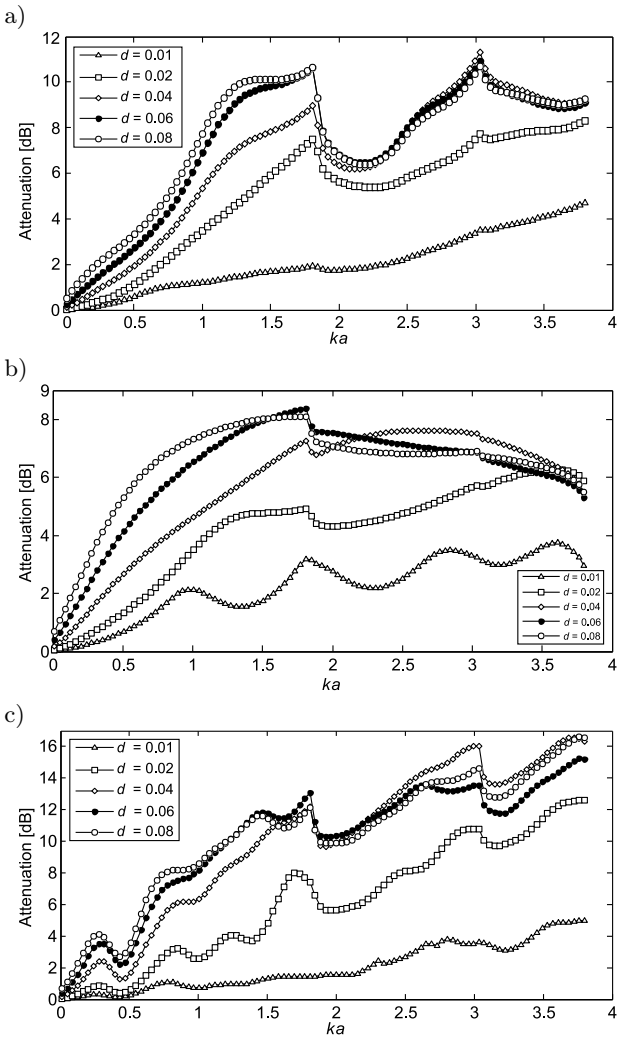

Fig. 16. Effect of the depth d [m] of the porous material on the acoustic power attenuation of the three studied configurations: a) (I-a), b) (I-b), and c) (I-c).

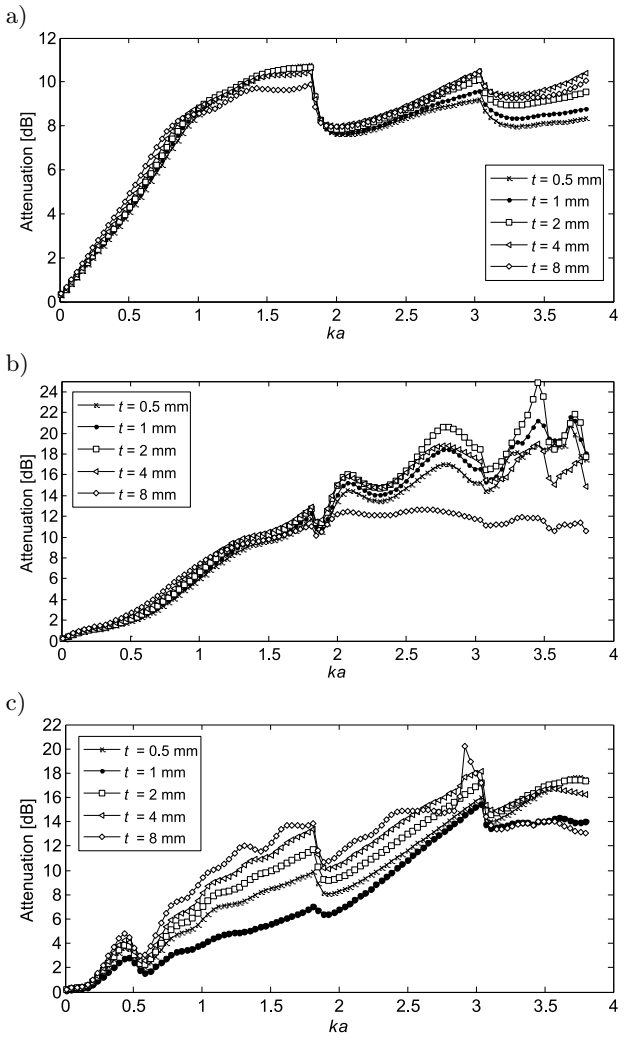

Fig. 17. Effect of the perforated plate thickness t on the acoustic power attenuation of the three studied configurations: a) (II-a), b) (II-b), and c) (II-c).

5.2.2. Configurations of ducts having an area widening

Plate characteristics effects. The effect of the plate thickness on the acoustic power attenuation of configurations (II-a), (II-b), and (II-c) are presented, respectively, in Fig. 17. These figures reveal that the results changed compared to those of Fig. 8, with regard to the cases of ducts having a radius narrowing. The acoustic behavior of each studied configuration can be described as follows: The acoustic power attenuation increases when ka increases, however, Fig. 17a shows drops at the mode cut-on frequencies. Moreover, perturbations of the attenuation are observed in Fig. 17b from ka above 2 and also a small fluctuation appears in Fig. 17c. This is explained by the fact that widening radius discontinuity creates evanescent waves that cause disturbances, when coupled with the propagating waves. By increasing the plate thickness from 0.5 to 8 mm, results show that this parameter has a negligible effect in configuration (a) for ka values less than 2.8 and it becomes low when ka is greater than 3, not exceeding 2 dB. Moreover, in configuration (b), the thickness has no effect up to ka = 2, where the attenuation starts to increase slightly with the thickness increase, except for t = 8 mm. The effect of plate thickness on configuration (II-c) is significant particularly at medium frequencies: the increase of this parameter generates an increase of the acoustic attenuation and its maximum passes from 7 dB for t = 1 mm to 14 dB for t = 8 mm at ka = 1.8. In each configuration, a maximum of attenuation is about: (II-a): 10.9 dB; (II-b); 25 dB; (II-c): 20 dB. It is noticeable that the results of these figures are more appropriate than the ones having radius narrowing. Therefore, the configurations of ducts having widening radius are more efficient than the three figures of a duct having a narrowing portion.

Figure 18 presents the effect of variation of the plate porosity σ_p on the acoustic power attenuation versus ka for the three studied configurations (II-a), (II-b), and (II-c). These figures show that the form

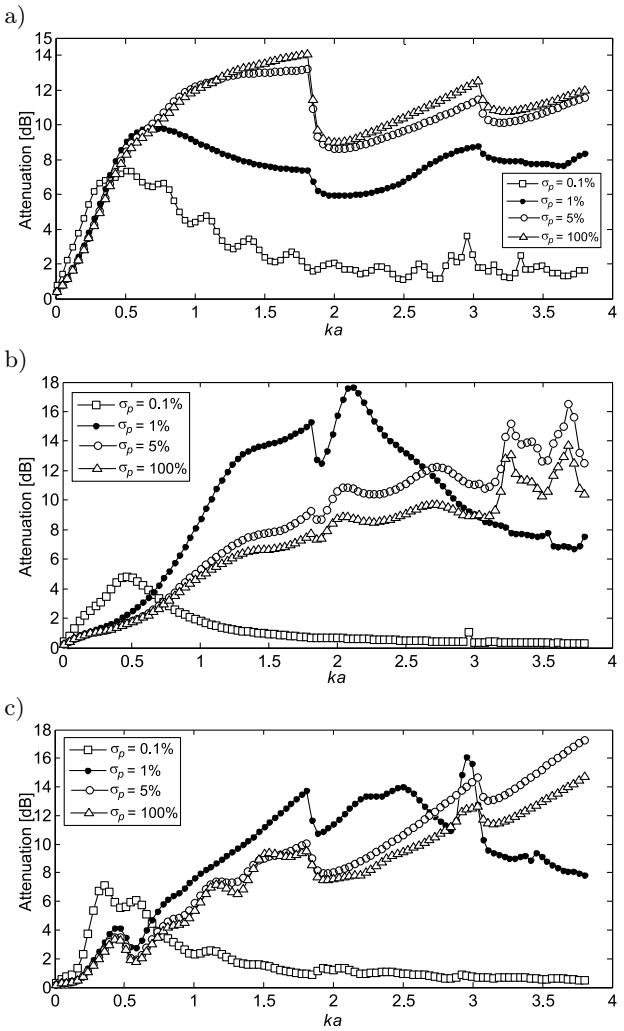

Fig. 18. Effect of the plate porosity on the acoustic power attenuation for the studied configurations: a) (II-a), b) (II-b), and c) (II-c).

of attenuation curves changes in each configuration, when σ_p = 0.1, 1%. The acoustic attenuation presents a peak at low frequencies range ka = [0.3, 0.8] for σ_p = 0.1% and then decreases until getting close to zero. For σ_p = 1%, the attenuation increases to reach a maximum equal 10 dB at ka = 0.6 and then slightly decreases, being equal to 8 dB at ka = 3.8. With regards to Figs 18b and 18c, the attenuation curves present a peak, exhibiting a maximum in the range of ka = [0.8, 2.65]. However, the acoustic power attenuation increases at the final point when ka rises for σ_p = 5, 10%. On the other hand, these attenuation curves are characterized by drops appearing in the mode cut-on frequencies for Fig. 18a and small disturbances for Figs 18b and 18c. The maximum of acoustic power attenuation changes for each figure: (a): 14 dB for σ_p = 5%; (b): 17.6 dB for σ_p = 1%; (c): 17.2 dB for σ_p = 5%. It is noticeable that the low values of σ_p have a great influence on the attenuation curves forms of each type of duct. It is found that the acoustic attenuation is better in configurations pertaining to the case of radius widening compared to the configurations related to the duct having a narrowing portion presented in Fig. 10. The maximum of attenuation changes from (II-a): 7.1 dB; (II-b): 10.97 dB; (II-c): 17.1 dB in the case of narrowing (Fig. 10) to (a): 17.8 dB; (b): 17.8 dB; (c): 17.1 dB in the case of widening. It is concluded that the widening radius of duct improves the acoustic attenuation by the reflection of acoustic waves into its discontinuity.

The effect of the plate hole diameter d_p on the acoustic power attenuation in the case of radius widening of ducts for different studied configurations are plotted in Figs 19a, 19b, and 19c, respectively, for configurations (II-a), (II-b), and (II-c). Results of these figures are close to that of the effect of porosity with small variations, manifested as follows: the attenuation increases until reaching a maximum about 5.6 dB, ka = 0.4 and 7.7 dB, ka = 0.5, respectively, for diameters 10 and 5 mm, then disturbances are observed, in Fig. 19a. On the other hand, such attenuation peaks slightly

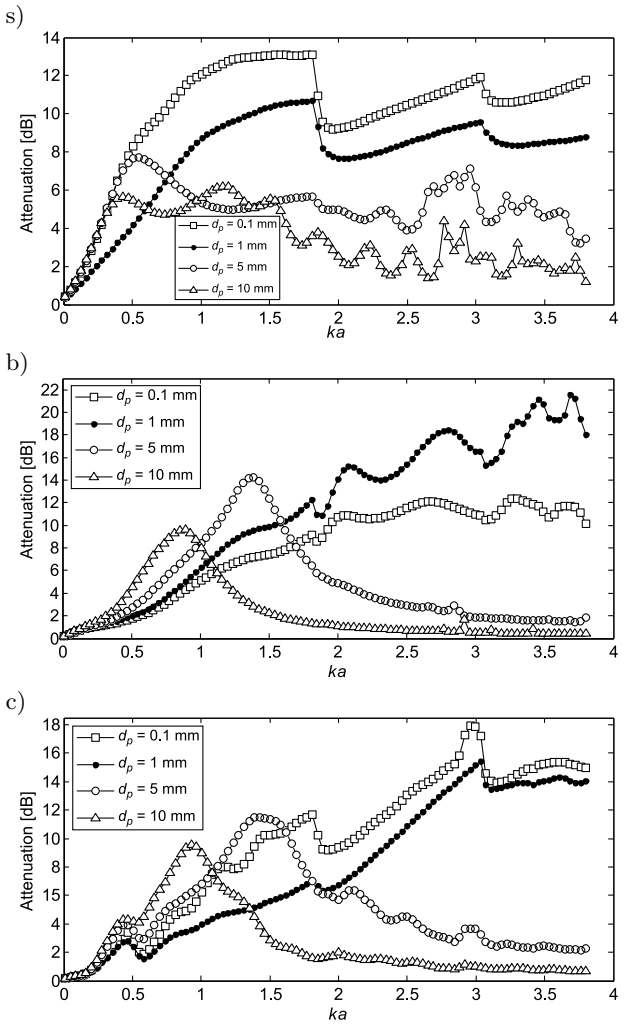

Fig. 19. Effect of the diameter d_p [mm] of the perforated plate on the acoustic power attenuation of the three studied configurations: a) (II-a), b) (II-b), and c) (II-c).

shift towards ka, being greater in Figs 19b and 19c. It is noted that the maximum attenuation is always given by smaller diameters values.

The results related to d_p = 0.1 mm are better in the entire frequency range in Fig. 19a, similarly for ka above 1.6 in Fig. 19c, and when d_p = 1 mm the results are rather good in Fig. 19b, for ka above 1.6. This is explained by the fact that the smaller the diameter is, the stronger the resistance of the plate is and thus leading to the attenuation increase. The maximum attenuation according the frequency change from each figure is (a): 13 dB, ka = 1.8 for d_p = 0.1 mm; (b): 21.5, ka = 3.6 for d_p = 1 mm; (c): 17.8 dB, ka = 3 for d_p = 0.1 mm. The comparison of the various models of the lined duct discontinuities suggests that the choice of d_p = 1 mm in configuration (II-b) is reasonable to improve the acoustic power attenuation.

Material porous properties effects. The effect of the flow resistivity on the acoustic power attenuation for configurations (II-a), (II-b), and (II-c) is plotted, respectively, in Figs 20a, 20b, and 20c. It is observed that the attenuation curves are almost identical for the values of σ = 1000 to 10 000 N·s/m^4 and the flow resistivity does not influence these values. However, the attenuation curves show an increase for σ = 50 000 and 100 000 N·s/m^4 from ka above 1.9, in Fig. 20a, and in the entire frequency range in Fig. 20c. It can be concluded that the variation of the flow resistivity has an influence only on high values. It is noted that configuration (II-b) presents a fluctuation, which increases for σ = 50000 N·s/m^4, however, it decreases for σ = 100 000 N·s/m^4. A maximum of attenuation according the frequency is observed for each configuration it is about: (II-a): 11.8 dB, ka = 3.8; (II-b): 21, ka = 3.7; (II-c): 10, ka = 1.9. As expected, Fig. 20c is the most efficient to reduce noise.

Figures 21–23 present respectively the effect of the variation of the thermal permeability, the tortuosity and the porosity of the porous material on the acoustic power attenuation versus ka, respectively, for the configurations (II-a), (II-b), and (II-c) for the case

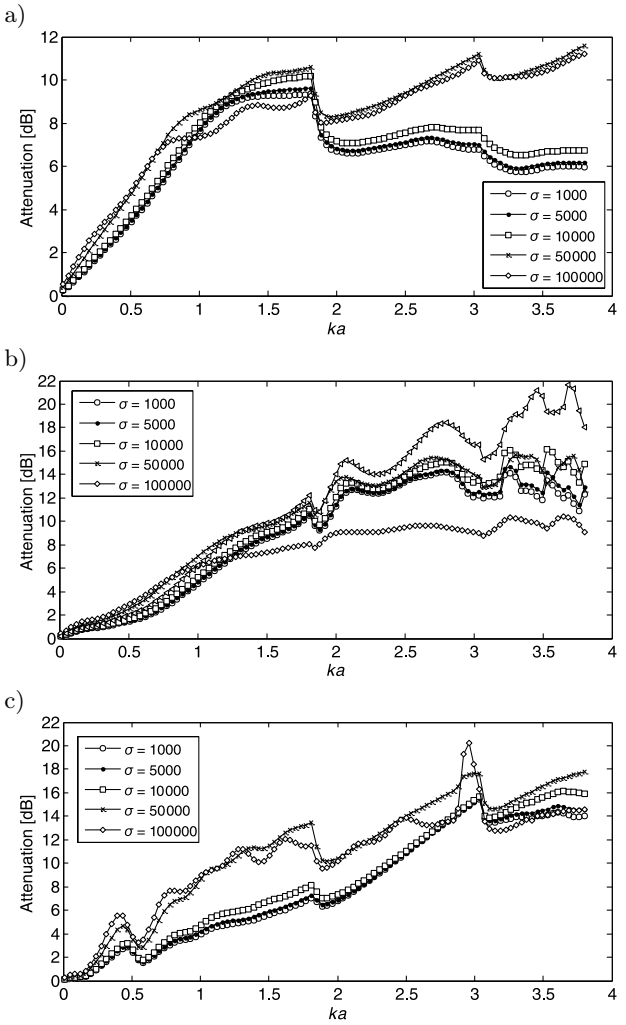

Fig. 20. Effect of the flow resistivity σ [N·m^{-1}·s] of the porous material on the acoustic power attenuation of the three studied configurations: a) (II-a), b) (II-b), and c) (II-c).

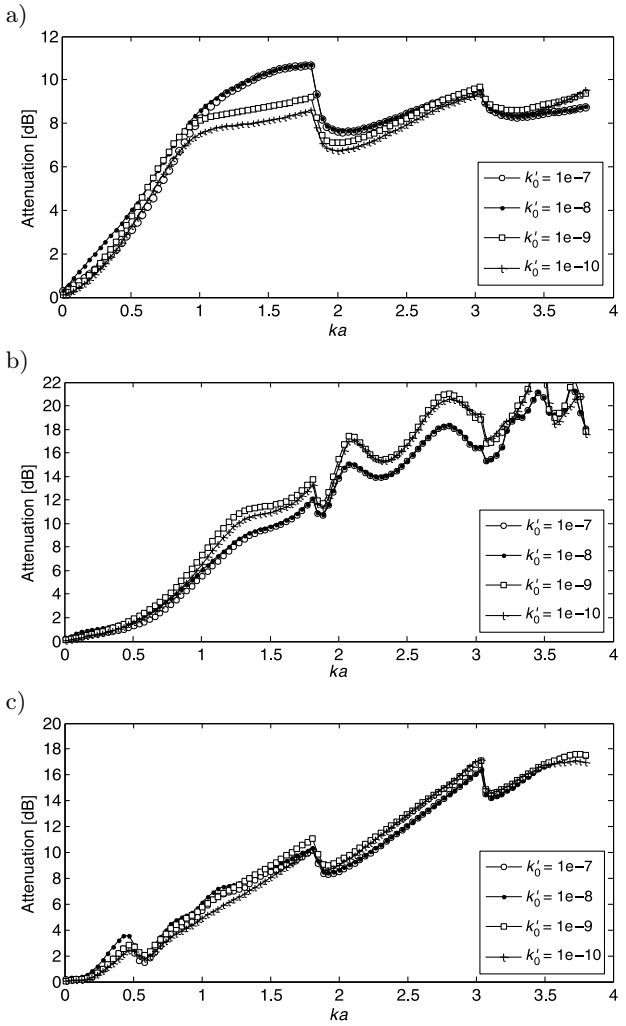

Fig. 21. Effect of the thermal permeability k_0' [m^2] of the porous material on the acoustic power attenuation of the three studied configurations: a) (II-a), b) (II-b), and c) (II-c).

widening of portion in duct. As expected, the influence of each of these parameters on the acoustic attenuation for each studied configuration is negligible. Except that for frequencies higher than ka = 3.1, in Figs 22b and 22c where the acoustic attenuation becomes disturbed and it decreases with the increase of the tortuosity. As well, in Fig. 23b, the attenuation grows with the increase of the porosity. It can be observed that the variation of the attenuation each those configuration (II-a), (II-b), and (II-c) is almost the same when varying each of the three parameters k_0', α_∞, and ϕ, but it changes a little when compared with configurations (I-a) and (I-b) in the case of a duct having radius narrowing. The acoustic behavior for all configurations of duct presenting widening of the radius can be described as follows: the acoustic power attenuation gradually grows when ka increases, but there are drops at the mode cut-on frequencies in configuration (II-a), a very small fluctuations are observed in configuration (II-b) which are more appears in Fig. 22b. The acoustic behavior in configuration (II-c) for the three porous

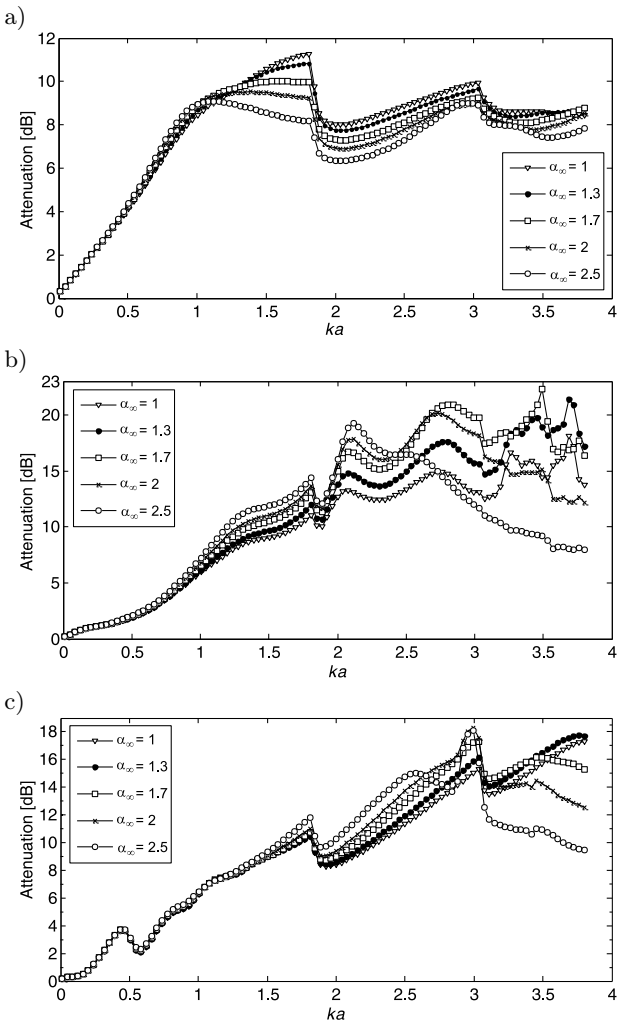

Fig. 22. Effect of the tortuosity α_∞ of the porous material on the acoustic power attenuation of ducts of the studied configurations: a) (II-a), b) (II-b), and c) (II-c).

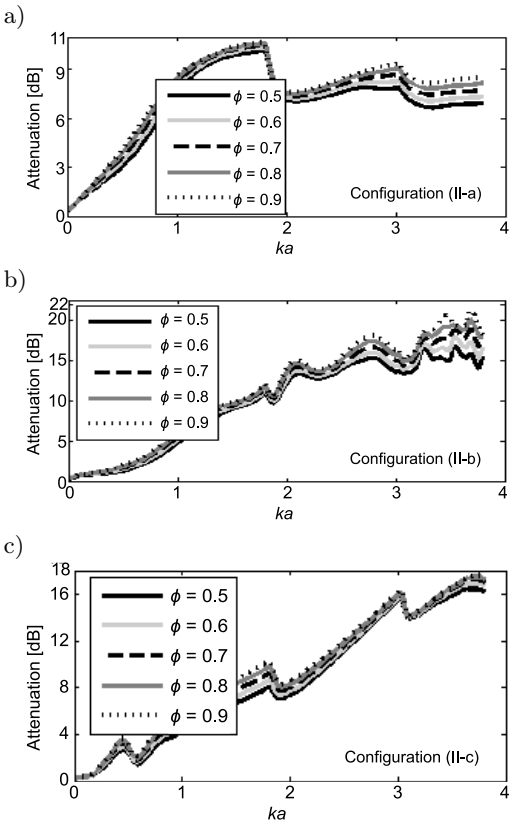

Fig. 23. Effect of the porosity ϕ of the porous material on the acoustic power attenuation of ducts with radius widening for the three studied configurations: a) (II-a), b) (II-b), and c) (II-c).

parameters k_0', α_∞, and ϕ is similar to that described for configuration (I-c) with small variation in Fig. 22c. It can be also seen that the attenuation is maximum for ka = 1.8 for configuration (II-a) and it reaches a maximum for ka ranging from 3.5 to 3.8 for configurations (II-b) and (II-c) as shown in Figs 21, 22, and 23.

For the thermal permeability, the attenuation levels are about 10.7 dB, 25 dB, and 17.5 dB for the (II-a), (II-b), and (II-c) configuration, respectively. It is clearly seen that the levels of attenuation for configurations of ducts having widening radius higher than that given in the case of duct with narrowing radius (I-a): 7.5 dB; (I-b): 9 dB; (II-c): 17 dB. For the tortuosity, it can be seen from Figs 22a, 22b, and 22c that the maximum of attenuation varies for each configuration (II-a): 11.2 dB; (II-b): 22.3 dB; (II-c): 18 dB. As expected, the results of a widening radius of ducts are better compared to those of the narrowing radius of ducts. Configuration (II-c) is a good choice because it yields good results, being less disturbed than configuration (II-b).

For the porosity, it is observed from Figs 23a, 23b, and 23c, a maximum of attenuation varies with respect to each configuration as follows: (II-a): 10.6 dB, ka = 1.8; (II-b): 21.2 dB, ka = 3.7; (II-c): 17.6 dB, ka = 3.8. Thus, configuration (II-c) yields the best results of the

greater attenuation, especially at high frequency and it is more efficient compared to the case of narrowing portion ducts (II-a): 11.8 dB; (II-b): 10 dB; (II-c): 15.4 dB.

Effect of the characteristics lengths of the porous material. The effect of the characteristic viscous length for all studied configurations (II-a), (II-b), and (II-c) is plotted in Fig. 24. It can be noticed from these figures that the attenuation curves for the values of Λ = 1e^{-3}, 1e^{-4} are almost confused with small variation, not stable for *ka* above 2, in Fig. 24b, and the variation of the acoustic power attenuation is similar to Fig. 15 in the case of narrowing portion. However, for the values of Λ = 1e^{-5}, 1e^{-6}, the forms of attenuation curves change. The attenuation slightly increases in the interval [0, 0.8] and then it represents fluctuations, which remain almost at the same level. The maximum of attenuation varies with respect to each configuration as follows: 10.8 dB, *ka* = 1.8 for (a); 25 dB, *ka* = 3.4 for (b); 17.7 dB, *ka* = 3.8 for (c). The results reveal that Fig. 24b, with a progressive discontinuity, is the most efficient in terms of improving the acoustic power attenuation, precisely at higher *ka* number.

Effect of the depth of the porous material. The effect of the depth of the porous material on the acoustic power attenuation for all studied configurations (II-a), (II-b), and (II-c) are plotted in Fig. 25. These figures reveal that the variation of the acoustic power attenuation is similar to Fig. 13 in the case of portion narrowing of the duct with small difference; however, the level of maximum attenuation is higher. The difference between the two cases is that Fig. 25a shows drops at the mode cut-on frequencies and disturbances of attenuation are observed in Fig. 25b. A maximum of attenuation according the frequency for each configuration is about: (II-a): 11.7 dB, *ka* = 3.8; (II-b), 16.8 dB, *ka* = 2.7; (II-c): 18 dB, *ka* = 3.8. The analysis of the effect of the depth of the porous material in all studied configurations reveals that configuration (II-c) in the case of widening portion duct is the most absorbent, with a diameter 0.08 mm, being the most efficient in the entire frequency range.

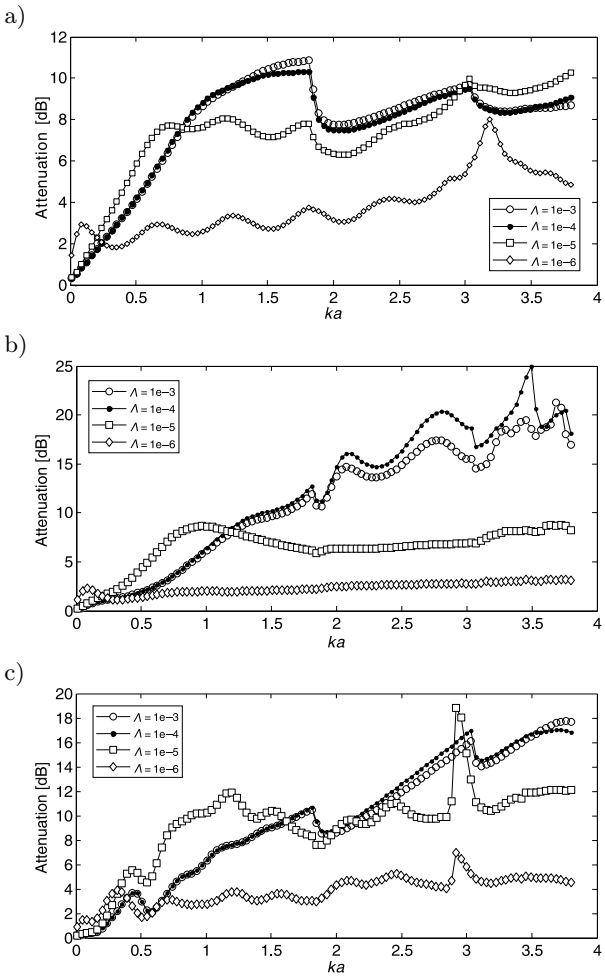

Fig. 24. Effect of the characteristic viscous length Λ [m] of the porous material on the acoustic power attenuation of the three studied configurations: a) (II-a), b) (II-b), and c) (II-c).

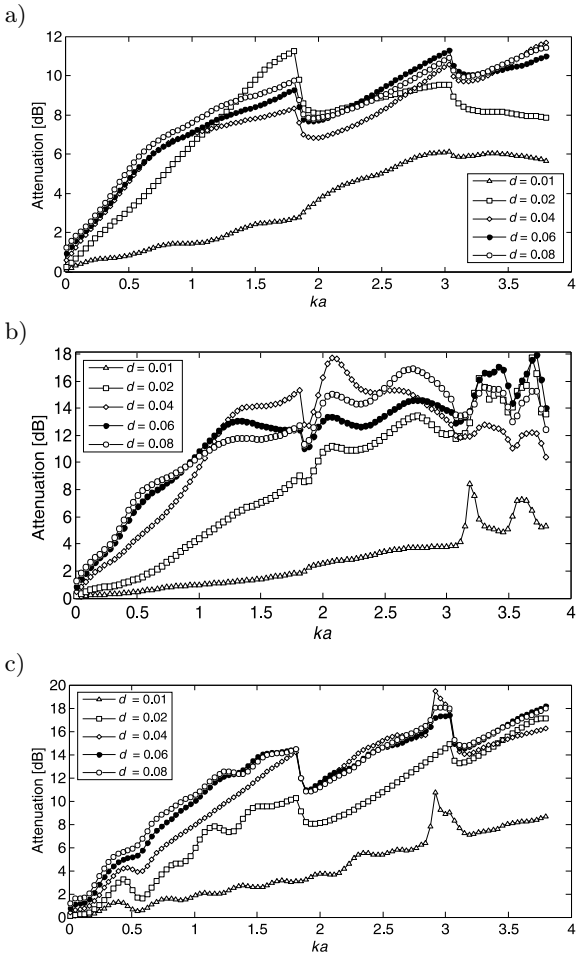

Fig. 25. Effect of the depth *d* [mm] of the porous material on the acoustic power attenuation of studied configurations: a) (II-a), b) (II-b), and c) (II-c).

6. Conclusion

In this work, the effect of variation of the liner parameters on the acoustic power attenuation of lined ducts discontinuities is performed using the multimodal scattering matrix computed numerically. In fact, this study is carried out based on six configurations to show the relative influence of discontinuities geometries and liner position in duct systems. The following primary conclusions are drawn from the results of this study:

- The results of effect of parameters of liner on the attenuation reveal that:
  - For the case of narrowing duct: the maximum of attenuation of configuration (I-b) is greater compared to that of configuration (I-a) (~2–4 dB), while it is less important for configuration (I-c), with a maximum of 5–8 dB.
  - For the cases of widening duct: configuration (II-a) is less important than those of configurations (II-b) and (II-c). The maximum attenuation is greater for configuration (II-b) (~4–11 dB) and configuration (II-c) (~4–7 dB) compared to that of configuration (a). It is noted that configuration (II-a) is not so effective for absorbing sound and therefore it is not preferable in the design of ducts systems.
- Among the various studied geometries, the case of widening duct is always better to increase the acoustic attenuation due to the reflection of the sound at the section discontinuities and more precisely in configurations (II-b) and (II-c), which yield the best results; however, these discontinuities cause disturbances of acoustic waves at high frequency range.
- The most influencing parameters of liner are those of the plate parameters and some parameters of porous material such as: Λ and d. Moreover, thickness t and flow resistivity σ have an influence only on some configurations.

The results presented in this work would be of great help as far the design of ducts and liner is concerned.

References

1. Åbom M.A. (1991), Measurement of the scattering matrix of acoustical two-ports, *Mechanical Systems Signal Processing*, **5**: 89–104, doi: 10.1016/0888-3270(91)90017-Y.
2. Akoum M., Ville J.M. (1998), Measurement of reflection matrix of a discontinuity in a duct, *The Journal of the Acoustical Society of America*, **103**(5): 2463–2468, doi: 10.1121/1.422766.
3. Amir N., Pagneux V., Kergomard J.A. (1996), A study of wave propagation in varying cross-section waveguides by modal decomposition. Part I. Theory and validation, *The Journal of the Acoustical Society of America*, **100**(4): 2034–2048, doi: 10.1121/1.417913.
4. Aurégan Y., Starobinski R. (1999), Determination of acoustical energy attenuation/production potentiality from the acoustical transfer functions of a multiport, *Acta Acustica united with Acustica*, **85**: 788–792.
5. Allard J.F., Attalla N. (1993), *Propagation of sound in porous media: Modeling sound absorbing materials*, Elsevier Applied Science, London 1993, 105–115.
6. Benjedidia M., Akrout A., Taktak M., Hammami L., Haddar M. (2014), Thermal effect on the acoustic behavior of an axisymmetric lined duct, *Applied Acoustics*, **86**: 138–145, doi: 10.1016/j.apacoust.2014.03.004.
7. Ben Souf M.A., Kessentini A., Bareille O., Taktak M., Ichchou M.N., Haddar M. (2017), Acoustical scattering identification with local impedance through a spectral approach, *Comptes Rendus Mécanique*, **345**(5): 301–316, doi: 10.1016/j.crme.2017.03.006.
8. Bi W.P., Pagneux V., Lafarge D., Aurégan Y. (2006), Modelling of sound propagation in non-uniform lined duct using a Multi-Modal Propagation Method, *Journal of Sound and Vibration*, **289**(4–5): 1091–1111, doi: 10.1016/j.jsv.2005.03.021.
9. Craggs A. (1989), The application of the scattering matrix and matrix condensation methods with finite elements to ducts acoustics, *Journal of Sound and Vibration*, **132**(3): 393–402, doi: 10.1016/0022-460X(89)90633-0.
10. Dhief R., Makni A., Taktak M., Chaabane M., Haddar M. (2020), Investigation on the effects of acoustic liner variation and geometry discontinuities on the acoustic performance of lined ducts, *Archives of Acoustics*, **45**(1): 49–66, doi: 10.24425/AOA.2020.132481.
11. Elnady T. (2004), *Modelling and characterization of perforates in lined ducts and mufflers* (Paper III), Doctoral Thesis, The Royal Institute of Technology (KTH), Stockholm, Sweden.
12. Kergomard J., Garcia A. (1987), Simple discontinuities in acoustic waveguides at low frequencies: critical analysis and formulae, *Journal of Sound and Vibration*, **114**(3): 465–479, doi: 10.1016/S0022-460X(87)80017-2.
13. Kessentini A., Taktak M., Ben Souf M.A., Bareille O., Ichchou M.N., Haddar M. (2016), Computation of the scattering matrix of guided acoustical propagation by the Wave Finite Elements approach, *Applied Acoustics*, **108**: 92–100, doi: 10.1016/j.apacoust.2015.09.004.
14. Lafarge D., Lemarinier P., Allard J.F., Tarnow V. (1997), Dynamic compressibility of air in porous structures at audible frequencies, *The Journal of Acoustical*

Society of America, **102**(4): 1995–2006, doi: 10.1121/1.419690.

15. Lee I., Selamet A. (2006), Impact of perforation impedance on the transmission loss of reactive and dissipative silencers, *The Journal of Acoustical Society of America*, **120**(6): 3706–3713, doi: 10.1121/1.2359703.
16. Leroux M., Job S., Aurégan Y., Pagneux V. (2003), Acoustical propagation in lined duct with flow. Numerical simulations and measurements, [in:] *10th International congress on Sound and Vibration*, Stockholm, Sweden, pp. 3255–3262.
17. Masmoudi A., Makni A., Taktak M., Haddar M. (2017), Effect of geometry and impedance variation on the acoustic performance of a porous material lined duct, *Journal of Theoretical and Applied Mechanics*, **55**(2): 679–694, doi: 10.15632/jtam-pl.55.2.679.
18. Miles J.W. (1946), The analysis of plane discontinuities in cylindrical tubes, Part I, *The Journal of the Acoustical Society of America*, **17**(3): 259–271, doi: 10.1121/1.1916327.
19. Mereze P.H., Becker R.P., Lenzi A., Pellegrini C. (2012), Rigid-Frame Porous Material Acoustic Attenuation on Compressor Discharge, [in:] *International Compressor Engineering Conference*, Paper 2095.
20. Munjal M.L. (2014), *Acoustics of Ducts and Mufflers*, 2nd ed., John Wiley & Sons Ltd., Chichester, UK, ISBN 978-1-118-44312-5.
21. Othmani C., Hentati T., Taktak M., Tamer E., Fakhfakh T., Haddar M. (2015), Effect of liner characteristics on the performance of duct systems, *Archives of Acoustics*, **40**(1): 117–127, doi: 10.1515/aoa-2015-0014.
22. Peat K.S. (1988a), The acoustical impedance at discontinuities of ducts in the presence of a mean flow, *Journal of Sound and Vibration*, **127**(1): 123–132, doi: 10.1016/0022-460X(88)90353-7.
23. Peat K.S. (1988b), The transfer matrix of a uniform duct with a linear temperature gradient, *Journal of Sound and Vibration*, **123**(1): 43–53, doi: 10.1016/S0022-460X(88)80076-2.
24. Selamet A., Xu M.B., Lee I.-J., Huff N.T. (2004), Analytical approach for sound attenuation in perforated dissipative silencers, *The Journal of the Acoustical Society of America*, **115**(5): 2091–2099, doi: 10.1121/1.1694994.
25. Sagartzazu X., Hervella-Nieto L., Pagalday J.M. (2008), Review in sound absorbing materials, *Archives of Computational Methods in Engineering*, **15**: 311–342.
26. Sitel A., Ville J.M., Foucart F. (2003), An experimental facility for measurement of acoustic transmission matrix and acoustic power dissipation of a duct discontinuity at higher modes propagation conditions, *Acta Acustica united with Acustica*, **89**(4): 586–594.
27. Sitel A., Ville J.M., Foucart F. (2006), Multimodal procedure to measure the acoustic scattering matrix of a duct discontinuity for higher order mode propagation conditions, *The Journal of the Acoustical Society of America*, **120**(5): 2478–2490, doi: 10.1121/1.2354040.
28. Taktak M., Ville J.M., Haddar M., Foucart F. (2008), Evaluation of a lined duct performance based on a 3D two port scattering matrix, *The Journal of the Acoustical Society of America*, **123**(5): 3926–3926, doi: 10.1121/1.2935966.
29. Taktak M., Ville J.M., Haddar M., Gabard G., Foucart F. (2010), An indirect method for the characterization of locally reacting liners, *The Journal of Acoustical Society of America*, **127**(6): 3548–3559, doi: 10.1121/1.3365250.
30. Taktak M., Majdoub M.A., Bentahar M., Haddar M. (2012), Numerical modelling of the acoustic pressure inside an axisymmetric lined flow duct, *Archives of Acoustics*, **37**(2): 151–160, doi: 10.2478/v10168-012-0021-8.
31. Tiryakioglu B. (2020), Radiation of sound waves by a semi-infinite duct with outer lining and perforated end, *Archives of Acoustics*, **45**(1): 77–84, doi: 10.24425/aoa.2020.132483.
32. Wang J., Rubini P., Qin Q. (2017), Application of a porous media model for the acoustic damping of perforated plate absorbers, *Applied Acoustics*, **127**(1): 324–335, doi: 10.1016/j.apacoust.2017.07.003.